

Translithospheric magma plumbing system of intraplate volcanoes as revealed by electrical resistivity imaging

Yabin Li¹, Aihua Weng^{1*}, Wenliang Xu², Zonglin Zou³, Yu Tang¹, Zikun Zhou¹, Shiwen Li¹, Yanhui Zhang⁴ and Guido Ventura^{5,6}

¹College of Geo-exploration Science and Technology, Jilin University, Changchun 130026, China

²College of Earth Sciences, Jilin University, Changchun 130061, China

³China Petroleum Pipeline Engineering Corporation, Langfang 065000, China

⁴Structure Health Monitoring and Control Institute, Shijiazhuang Tiedao University, Shijiazhuang 050043, China

⁵Istituto Nazionale di Geofisica e Vulcanologia, Via di Vigna Murata 605, 00143 Roma, Italy

⁶Istituto per lo Studio degli Impatti Antropici e Sostenibilità in Ambiente Marino, Consiglio Nazionale delle Ricerche (CNR), Capo Granitola (TP), 91021 Campobello di Mazara, Italy

ABSTRACT

The magma plumbing systems of volcanoes in subduction and divergent tectonic settings are relatively well known, whereas those of intraplate volcanoes remain elusive; robust geophysical information on the magma pathways and storage zones is lacking. We inverted magnetotelluric data to image the magma plumbing system of an intraplate monogenetic volcanic field located above the stagnant Pacific slab in northeast China. We identified a complex, vertically aligned, low-resistivity anomaly system extending from the asthenosphere to the surface consisting of reservoirs with finger- to lens-like geometries. We show that magma forms as CO₂-rich melts in a 150-km-deep asthenospheric plume crossing the whole lithosphere as hydrated melt, inducing underplating at 50 km depth, evolving in crustal reservoirs, and erupting along dikes. Intraplate volcanoes are characterized by low degrees of melting and low magma supply rates. Their plumbing systems have a geometry not so different from that of volcanoes in subduction settings.

INTRODUCTION

Volcanoes on Earth are concentrated along subduction zones, mid-ocean ridges, and continental rifts. Volcanism in intraplate settings is poorly understood and is interpreted as the result of mantle melting processes induced by the rising of hot plumes or by the release of fluids from stagnant slabs (Chen et al., 2017). The magma plumbing systems of intraplate monogenetic volcanoes above stagnant slabs are enigmatic and lack robust geophysical constraints. In particular, the full magma pathway from the asthenosphere to the surface as well as the size and geometry of the storage zones are poorly known (Smith and Németh, 2017). Northeast China has monogenetic volcanic fields such as the Jingpohu monogenetic volcanic field (JMVF) and a metasomatized mantle plume located above the ~500-km-deep stagnant Pacific slab (Figs. 1A–1D; Chen et al., 2017; Li et al., 2020b). We obtained well-resolved

images of the JMVF magma plumbing system from a depth of ~150 km to the surface by inverting magnetotelluric (MT) data, which are useful in identifying magma storage zones below volcanoes (Hill et al., 2009; Comeau et al., 2015). Data were collected from an array of MT stations centered on the JMVF (Fig. 1E). We recognized a complex resistivity pattern below the JMVF. The observed anomalies, integrated with rock-physics models, provide a well-constrained picture of the structure of the plumbing system of a monogenetic volcanic field from the asthenosphere to the surface. Our results at the JMVF provide new insights into the geometry, size, and depth of magma reservoirs for volcanoes in intraplate settings (Smith and Németh, 2017).

GEOLOGIC SETTING

JMVF activity mainly developed in the Pleistocene and Holocene, with the last eruptions occurring in historical times (2470 and 3940 yr B.P.; Wei et al., 2003). The JMVF vents follow

two main alignments: a large-scale northeast-southwest alignment and a local north-south alignment (Fig. 1F). The northeast-southwest alignment is controlled by the left-lateral, ENE-WSW- to northeast-southwest-striking Dunhua-Mishan fault (DMF) system, which affects the entire crust and the mantle to depths of 35–40 km (Xu et al., 2017). The Yilan-Yitong fault (YIF) system is located north of the JMVF and bounds the Songliao sedimentary basin. The JMVF eruptions produced ~2 km³ of basaltic, trachybasaltic and basaltic lava flows and scorias. The compositions of basalts record mixing between enriched mantle 1 (EM1) and depleted mantle (DM) sources and contamination by lower-crust material (Zhang et al., 2000; Yan and Zhao, 2008). The alkaline volcanism of northeast China, including the JMVF, involved carbonate melts (C melts) supplied from the mantle transition zone (MTZ) by the eclogites in the stagnant Pacific slab and peridotites associated with the overlying mantle wedge (Figs. 1B–1D; Xu et al., 2020; Zhang et al., 2020).

MAGNETOTELLURIC DATA AND MODELING

Magnetotelluric data were collected using nine long-period MT (LMT) and 31 broadband MT (BBMT) stations (Fig. 1E) arranged around the JMVF. We deployed 25 BBMT instruments in a grid with an average spacing of ~33 km. In the central area, six BBMT stations were added to the network to better constrain the crust structure beneath the JMVF. The BBMT data were collected using a minimum acquisition time of

*E-mail: wengaihua@sina.com

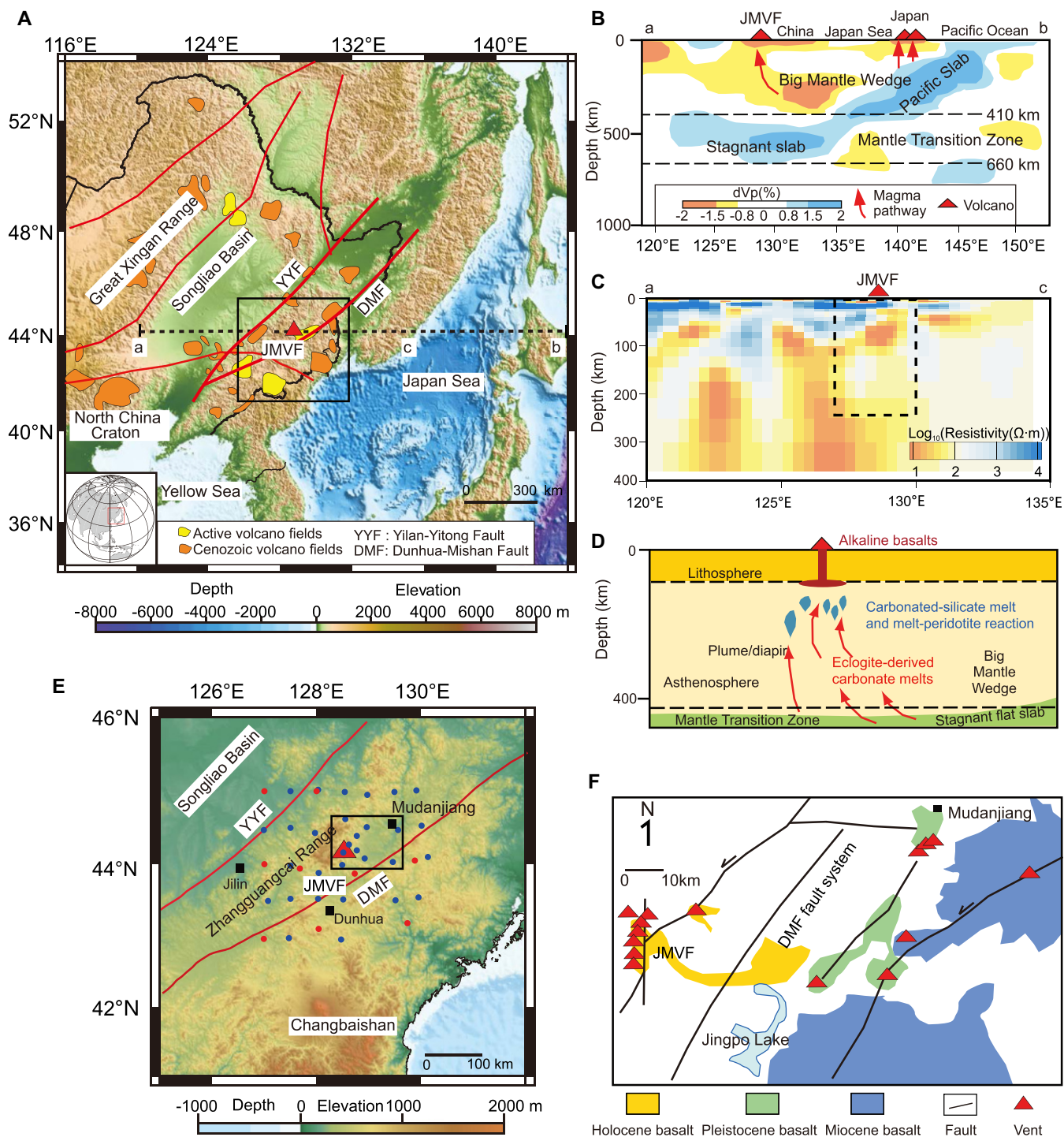


Figure 1. Tectonic setting of northeast China and the structural scheme of the Jingpohu monogenetic volcanic field (JMVF) area. (A) Distribution of volcanism and major tectonic structures in northeast China. (B) Location of high- and low- V_p anomalies along profile a–b in A (modified from Ma et al., 2019). (C) Resistivity model along profile a–c in A (modified from Li et al., 2020b). (D) Schematic illustration of petrological model for northeast China magmatism modified from Xu et al. (2020) and Zhang et al. (2020). (E) Location of JMVF area and distribution of magnetotelluric (MT) stations (LMT—long-period MT; BBMT—broadband MT). Box around the JMVF outlines the area of JMVF geologic map in F. Volcanic fields are marked with red triangles. (F) Simplified geologic map of JMVF area (modified from Zhang et al., 2000).

20 h and processed to obtain full impedance with periods from ~ 0.003 s to 2000 s, while >20 d LMT data had responses with periods from 10 s to $\sim 20,000$ s. Representative apparent resistivity and phase curves of off-diagonal and full-impedance tensors around JMVF are reported in Figures S1 and S2, respectively, in the

Supplemental Material¹. A three-dimensional,

¹Supplemental Material. Details on the 3-D magnetotelluric inversion, sensitivity test of resistivity anomalies and melt fraction estimation, and Figures S1–S11. Please visit <https://doi.org/10.1130/GEOLOGY.14903307> to access the supplemental material, and contact editing@geosociety.org with any questions.

nonlinear, conjugate-gradient inversion technique was applied to convert the MT responses to resistivity images from data sets including off-diagonal and full-impedance tensors. Compared to the off-diagonal impedance inversion model, the full-impedance inversion model showed a more complicated resistivity pattern

at crustal depth (Fig. S3), likely due to some distortion of diagonal impedances by noise (Fig. S2). As the two prominent anomalies in the mantle are key to understanding the deep structure below JMVF, we preferred the inversion model from off-diagonal impedances. Selection of this model also considered the facts that the fitting of the full-impedance tensor was not satisfactory, that of off-diagonal data was good (Fig. S1), and the diagonal component was often significantly smaller than the off-diagonal impedance (e.g.,

curve on site 47 in Fig. S2). Details on the data elaboration, inversion methods, evaluation of the quality of the inversion from off-diagonal impedance tensor data, and sensitivity analysis are provided in the Supplemental Material and Figures S4–S9.

RESULTS

Figure 2 shows the resistivity structure of the JMVF and surrounding area. The anomaly pattern is characterized by deep-rooted, vertically

aligned, low-resistivity zones in the mantle and shallower anomalies at the Moho and in the crust. From the surface to ~ 20 km depth, the crust beneath the JMVF is generally highly resistive, with resistivity values up to $\sim 10^4 \Omega\cdot\text{m}$ (anomaly R in Figs. 2D and 2E). These values are consistent with the occurrence of the Precambrian and Paleozoic plutonic rocks of the Zhangguangcai Range (Xu et al., 2017). Localized sheet-like low-resistivity anomalies also exist, which are mostly distributed along the

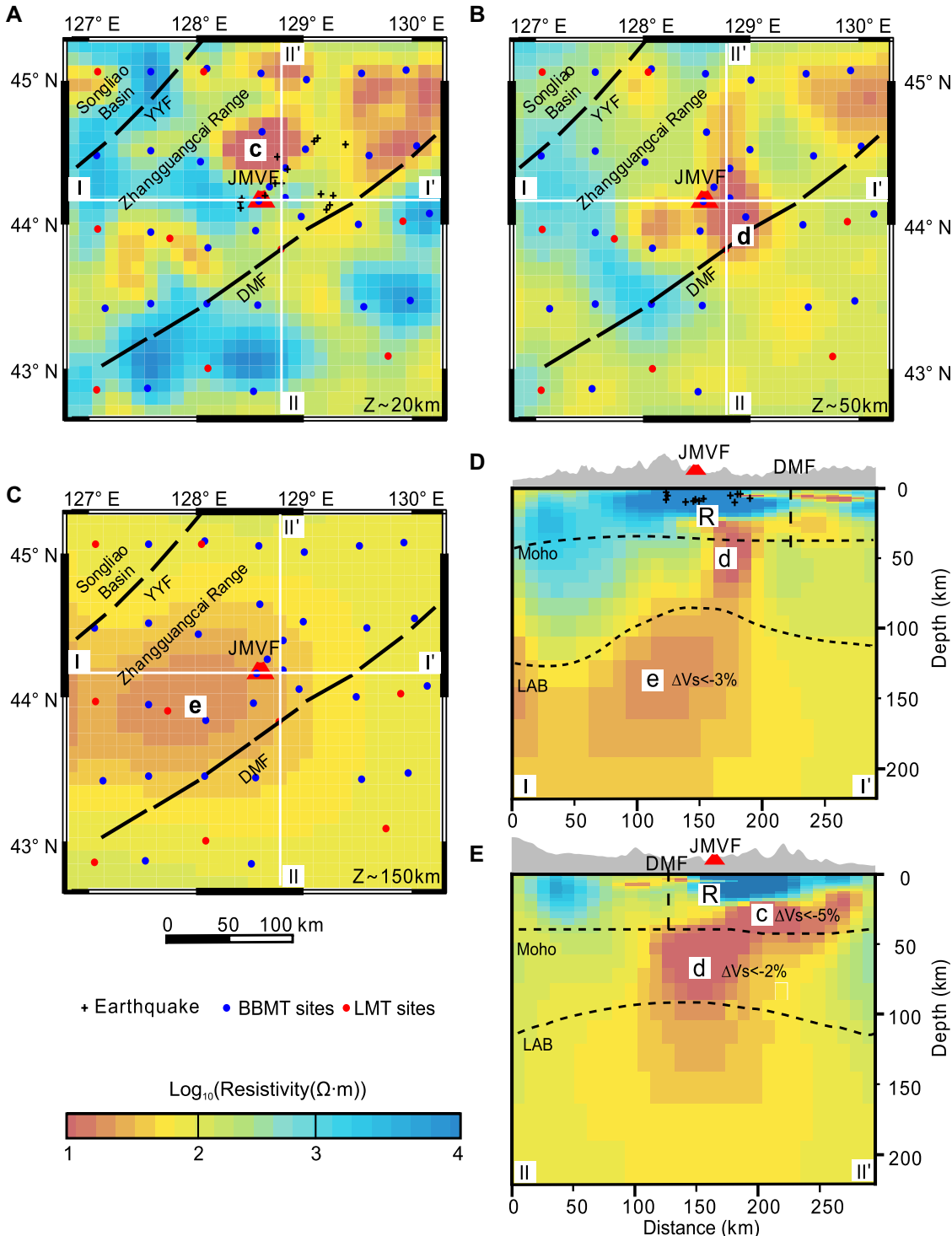


Figure 2. Magnetotelluric resistivity images beneath the Jingpohu monogenetic volcanic field (JMVF, northeast China). Slices are at depths of (A) 20 km, (B) 50 km, and (C) 150 km below sea level. (D,E) Cross sections along profiles I-I' (D) and II-II' (E). Anomalies are marked by bold letters R, c, d, and e. Earthquakes were recorded from January 2009 to December 2020. Magnitude (M_s) was between 0.1 and 1.8 (data from <http://data.earthquake.cn>). Depths of the Moho and lithosphere-asthenosphere boundary (LAB) in D and E were inferred from Xu et al. (2017) and Yan and Zhao (2008), respectively. Velocity perturbations in anomaly e in D are from Kang et al. (2016), while those in anomalies d and c in E refer to Fan and Chen (2019) and Pang et al. (2016), respectively. DMF—Dunhua-Mishan fault; YYF—Yilan-Yitong fault; LMT—long-period magnetotelluric data; BBTM—broadband magnetotelluric data.

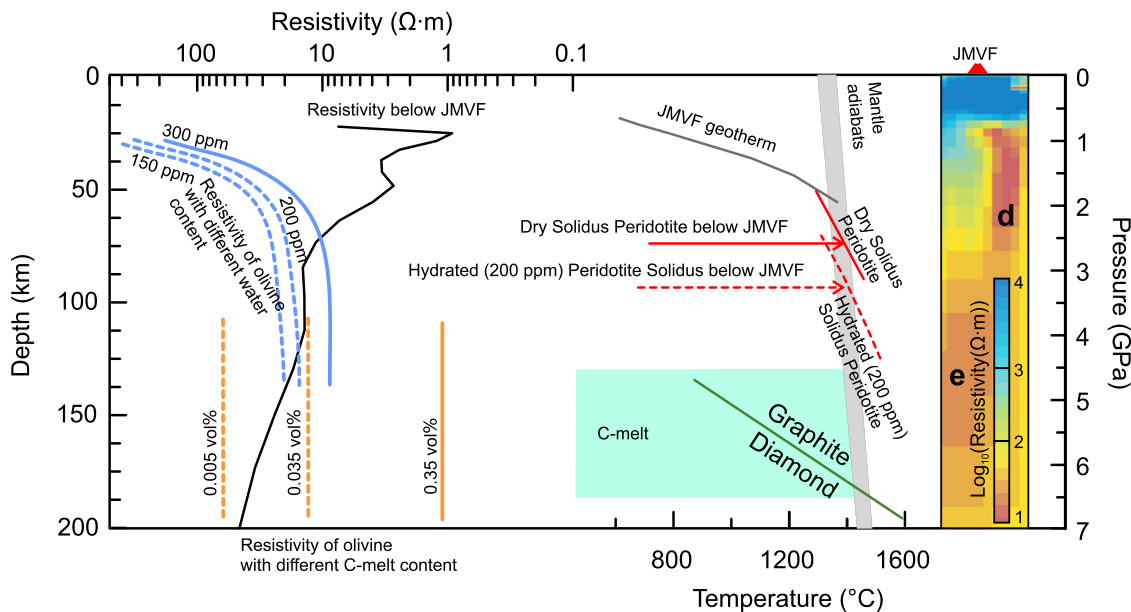


Figure 3. Rock physics interpretation of resistivity anomalies. Black line is resistivity depth profile beneath the Jingpohu monogenetic volcanic field (JMVF, northeast China) extracted from the right panel, where anomalies d and e are labeled by bold letters. Resistivities (blue lines) of olivine containing H₂O are from Gardés et al. (2014) along mantle adiabat (gray zone field); from Fischer et al., 2010). Resistivities of olivine with carbonate melt (brown lines) are from Gaillard et al. (2008). Geotherm beneath the JMVF was extrapolated from Fischer et al. (2010) with heat flow of ~90 mW/m² (An and Shi, 2007). Solidus (red lines) of dry and 200 ppm hydrated perido-

tite is from Hirschmann et al. (2009) according to geotherm beneath the JMVF. Azure area marks depths where conductivity is dominated by carbonate (C) melts, and the line represents stability fields of graphite and diamond from Fischer et al. (2010).

DMF at depths of 10–15 km (Figs. 2D and 2E), reflecting the presence of intracrustal fluid-rich zones, the depths of which are possibly controlled by crustal discontinuities (Wannamaker et al., 2009). A low-resistivity zone (anomaly c in Figs. 2A and 2E) is observed between depths of 20 and 40 km. This ~50-km-wide anomaly is located to the north of the JMVF in the middle-lower crust. The average resistivity is ~2–3 Ω · m, but in the central part, it is characterized by values <1 Ω · m (Fig. S3). Below the JMVF, an up to 50–70-km-wide, low-resistivity anomaly, anomaly d (~20 Ω · m), extends down to the lithosphere-asthenosphere boundary at a depth of ~75 km (Figs. 2B, 2D, and 2E; Yan and Zhao, 2008). At depths of ~130 km, the mantle becomes less resistive than 25 Ω · m in a spindle-like zone slightly tilted upward to anomaly d. We defined this low-resistivity zone as anomaly e (Figs. 2C and 2D). It probably represents the top of an up to 400-km-deep, low-resistivity anomaly detected in the asthenosphere (Fig. 1C; Li et al., 2020b). In its central area, the resistivity becomes as low as 15 Ω · m. In this moderately resistive situation, the 20,000 s period of our LMT data is sufficient to guarantee such a depth of investigation. The resistivity of the anomalies detected must be interpreted with some caution because MT data are primarily sensitive to the integrated conductance of conductive bodies. However, the inversions with identical data coverage to real observations demonstrate that the detected anomalies at depths from 20 km to 150 km are resolved rather well (Fig. S6). The robustness of the single anomaly described above is demonstrated by the results of model perturbation analysis (Figs. S8 and S9).

DISCUSSION

Anomaly e in the asthenosphere may be ascribed to high-temperature carbonate melts, peridotite, and/or hydrated melts in the asthenosphere (Fig. 3). Producing this low-resistivity anomaly with only high temperatures requires temperatures as high as ~1800 K (Gardés et al., 2014), which are incompatible with the pressure and temperature conditions for peridotite melts (~1500 K) and exceed the mantle adiabat (~1600 K). Alternatively, we can use olivine containing ~200 ppm H₂O to interpret the observed resistivity. However, such a high water content corresponds to ~700–1000 ppm H₂O in peridotite, i.e., well above the mantle water storage capacity (Hirschmann et al., 2009); in addition, this range of H₂O contents is not consistent with the relatively dry source(s) of the JMVF and northeast China basalts (Hsu and Chen, 1998). These difficulties lead us to associate anomaly e with C melts (Gaillard et al., 2008), where ~0.03 vol% of interconnected C melts may reproduce the observed resistivity values (Fig. 3). The reduction in S-wave velocity (Fig. 2D; Kang et al., 2016) in correspondence with anomaly e could reflect the occurrence of such melts. Results from the MAGLAB platform (Massuyeau et al., 2021) suggest a melt with ~300 ppm CO₂ and 240 ppm H₂O for anomaly e (Fig. S10). The widespread mantle-derived CO₂ around the JMVF area (Liu et al., 2018), the experimental petrological data on the stability of C melts (Zhang et al., 2020), the presence of alkali olivine basalts (Zhang et al., 2000), and the available isotopic data (⁸⁶Mg values of -0.6‰ to -0.30‰ in basalts) (Li et al., 2017) support our interpretation. Anomaly e

thus represents a volume where C melts occur beneath intraplate volcanoes, a feature mainly observed in divergent geodynamic contexts (Key et al., 2013; Sifré et al., 2014). C melts from the asthenosphere ascend across their stability field at a depth of ~120 km (Key et al., 2013; Sifré et al., 2014). Consequently, the low resistivity of anomaly d, originating from a depth of ~100 km, should be ascribed not only to C melts (Key et al., 2013) but also to peridotite partial melting (Yan and Zhao, 2008) triggered by ~200 ppm H₂O (Fig. 3; Hirschmann et al., 2009). The melting in anomaly d may be only ~1–2 vol% with a relatively low water content (1–2 wt%; Fig. S11; Hsu and Chen, 1998), and the low resistivity at the top of anomaly d suggests magma accumulation at the base of the crust, which could explain the ~2%–3% seismic velocity decrease (Fig. 2E; Fan and Chen, 2019). In the central sector, anomaly d shows a resistivity of 2–3 Ω · m, a value suggesting ~10 vol% of melt in its core (Fig. S11). The anomalies detected below the JMVF suggest, on average, low melting fractions (4–6 vol%) and water contents (<1.5 wt%). These values are significantly lower than the up to 12 vol% melting fraction and 2.5–9 wt% water content of the sources feeding the volcanoes in subduction settings (Comeau et al., 2015; Laumonier et al., 2017).

Therefore, anomaly d represents the mantle source of the JMVF basalts. In this scenario, the EM1 component of the JMVF basalts (Hsu and Chen, 1998) could be lithospheric, thermally eroded underplated material (Konter and Becker, 2012), implying active underplating processes. In the JMVF, ~2 km³ of basaltic lavas erupted

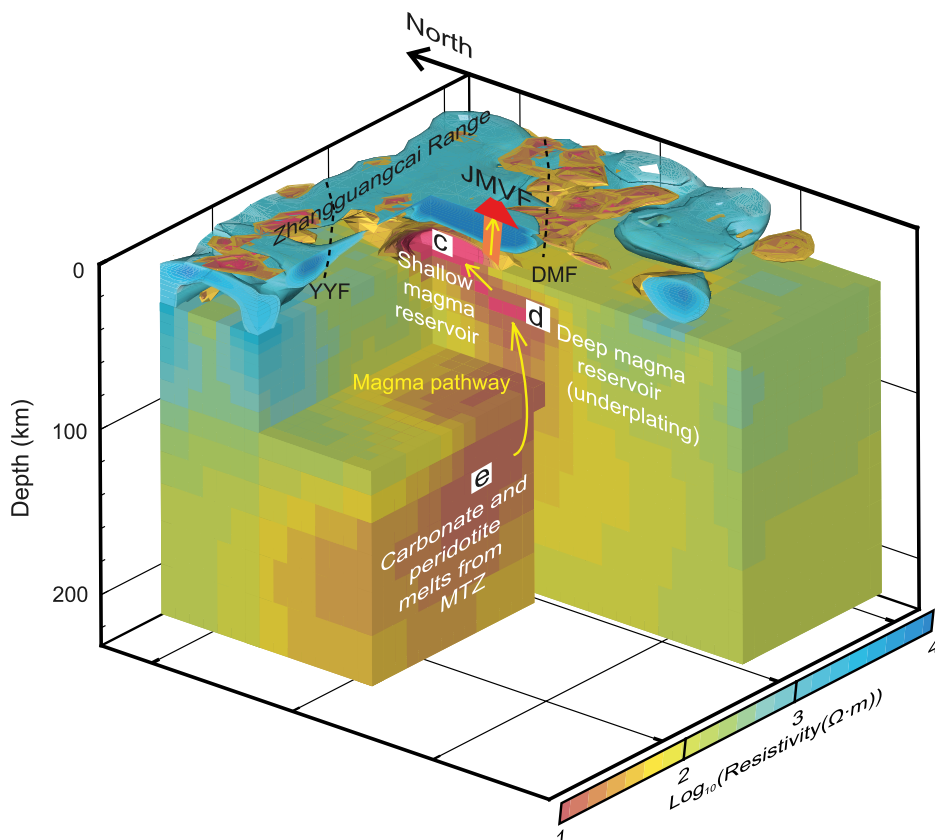


Figure 4. Conceptual model of the Jingpohu monogenetic volcanic field (JMVF, northeast China) intraplate plumbing system based on inversion of magnetotelluric data. Magma pathways are marked by yellow arrows. Bold c, d, and e indicate resistivity anomalies. Structural and volcanological significance of three main magma storage zones are discussed in text. DMF—Dunhua-Mishan fault; YYF—Yilan-Yitong fault; MTZ—mantle transition zone.

from the source in ~ 8000 yr (Yan and Zhao, 2008), equal to an average magma production rate of 2.5×10^{-4} km³/yr, a value within the 10^{-5} – 10^{-3} km³/yr range estimated for alkaline volcanoes in intraplate settings and significantly lower than that of subduction volcanoes (0.4–0.6 km³/yr; Crisp, 1984). We suggest that the JMVF magmatic system is characterized by a high ratio between intrusions and erupted products. This observation and the low melt fraction and water content of the JMVF reservoirs may explain why the magma production rate of intraplate volcanoes is lower than that of volcanoes in subduction settings. The low-resistivity midcrust anomaly c is located just above anomaly d. We interpret anomaly c as the shallow magma reservoir of the JMVF. This reservoir could have been the source of the andesitic magma erupted in the Eocene (Qin et al., 2008). The 1–2 Ω -m bulk resistivity of anomaly c implies an ~ 10 vol% melt with 2.5 wt% water (Li et al., 2020a). The presence of this midcrustal hot melting zone is supported by (1) a low-velocity zone in the same region (Fig. 2E; Pang et al., 2016), (2) an ~ 100 kg/m³ density decrease at 20–30 km below the JMVF (Suo et al., 2015), and (3) the occurrence of seismicity confined to the upper 12 km of the crust (Fig. 2D). The hypocentral

depths suggest a brittle-ductile transition shallower than the ~ 20 km depth expected for an intraplate setting with underlying Paleozoic basement (Xu et al., 2017). This could reflect the thermal anomaly associated with the low-resistivity anomaly c. Although the conduits for eruptions cannot be seen in our image due to the large instrument spacing, transcrustal magma transfer can occur, according to field data, along the dikes associated with major faults (Xu et al., 2017).

Our results reveal the multilevel structure of the JMVF plumbing system, which is characterized by (Fig. 4): (1) a deeper zone located in the asthenospheric mantle fed by a C-melt-rich plume, possibly ascending from the MTZ above the stagnant Pacific slab (Ma et al., 2019; Xu et al., 2020); (2) an intermediate storage zone extending from the upper mantle to the Moho, in which hydrated peridotite melts form and underplating processes develop; (3) a shallower, intracrustal reservoir; and (4) a surface, fault-guided dike system responsible for the alignment of monogenetic vents. With the exception of the asthenospheric mantle zone, this configuration is unexpectedly very similar to that of silicic stratovolcanoes typical of arc settings (Afanasyev et al., 2018).

CONCLUSIONS

Our study reveals the complete architecture of the magma plumbing system of an intraplate volcanic field above a stagnant slab. Our results suggest that the main differences between silicic, mainly explosive subduction volcanism and lower-energy, basaltic intraplate volcanism are related to the low water content and melt fraction of the mantle above stagnant slabs and not to the geometry of the plumbing system. Our data highlight the role of C melts and poorly hydrated silicate melts in the formation of magma reservoirs beneath intraplate volcanoes.

ACKNOWLEDGMENTS

We thank G. Egbert for sharing his ModEM package codes. We are grateful to Denghai Bai, Xiangyun Hu, and V. Sepe for critical discussions. We are grateful for the computational resources from Jilin Kingti Geoexploration Tech, Ltd. (Changchun, China). This work was supported by the National Natural Science Foundation of China (grants 42074080 and 91858211) and Istituto Nazionale di Geofisica e Vulcanologia (Italy) funds to G. Ventura. We gratefully acknowledge editor Chris Clark for handling, and Hanchao Jian, Fabrice Gaillard, and an anonymous reviewer for manuscript reviews.

REFERENCES CITED

- Afanasyev, A., Blundy, J., Melnik, O., and Sparks, S., 2018, Formation of magmatic brine lenses via focussed fluid-flow beneath volcanoes: Earth and Planetary Science Letters, v. 486, p. 119–128, <https://doi.org/10.1016/j.epsl.2018.01.013>.
- An, M.J., and Shi, Y.L., 2007, Three-dimensional thermal structure of the Chinese continental crust and upper mantle: Science in China, Earth Sciences, v. 50, p. 1441–1451, <https://doi.org/10.1007/s11430-007-0071-3>.
- Chen, C., Zhao, D., Tian, Y., Wu, S., Hasegawa, A., Lei, J., Park, J.H., and Kang, I.B., 2017, Mantle transition zone, stagnant slab and intraplate volcanism in Northeast Asia: Geophysical Journal International, v. 209, p. 68–85, <https://doi.org/10.1093/gji/ggw491>.
- Comeau, M.J., Unsworth, M.J., Ticona, F., and Sunagua, M., 2015, Magnetotelluric images of magma distribution beneath Volcán Uturuncu, Bolivia: Implications for magma dynamics: Geology, v. 43, p. 243–246, <https://doi.org/10.1130/G36258.1>.
- Crisp, J.A., 1984, Rates of magma emplacement and volcanic output: Journal of Volcanology and Geothermal Research, v. 20, p. 177–211, [https://doi.org/10.1016/0377-0273\(84\)90039-8](https://doi.org/10.1016/0377-0273(84)90039-8).
- Fan, X., and Chen, Q.F., 2019, Seismic constraints on the magmatic system beneath the Changbaisan volcano: Insight into its origin and regional tectonics: Journal of Geophysical Research: Solid Earth, v. 124, p. 2003–2024, <https://doi.org/10.1029/2018JB016288>.
- Fischer, K.M., Ford, H.A., Abt, D.L., and Rychert, C.A., 2010, The lithosphere-asthenosphere boundary: Annual Review of Earth and Planetary Sciences, v. 38, p. 551–575, <https://doi.org/10.1146/annurev-earth-040809-152438>.
- Gaillard, F., Malki, M., Iacono-Marziano, G., Pichavant, M., and Scaillet, B., 2008, Carbonatite melts and electrical conductivity in the asthenosphere: Science, v. 322, p. 1363–1365, <https://doi.org/10.1126/science.1164446>.
- Gardés, E., Gaillard, F., and Tarits, P., 2014, Toward a unified hydrous olivine electrical

- conductivity law: *Geochemistry Geophysics Geosystems*, v. 15, p. 4984–5000, <https://doi.org/10.1002/2014GC005496>.
- Hill, G.J., Caldwell, T.G., Heise, W., Chertkoff, D.G., Bibby, H.M., Burgess, M.K., Cull, J.P., and Cas, R.A.F., 2009, Distribution of melt beneath Mount St. Helens and Mount Adams inferred from magnetotelluric data: *Nature Geoscience*, v. 2, p. 785–789, <https://doi.org/10.1038/ngeo661>.
- Hirschmann, M.M., Tenner, T., Aubaud, C., and Withers, A.C., 2009, Dehydration melting of nominally anhydrous mantle: The primacy of partitioning: *Physics of the Earth and Planetary Interiors*, v. 176, p. 54–68, <https://doi.org/10.1016/j.pepi.2009.04.001>.
- Hsu, C.N., and Chen, J.C., 1998, Geochemistry of late Cenozoic basalts from Wudalianchi and Jingpohu areas, Heilongjiang Province, Northeast China: *Journal of Asian Earth Sciences*, v. 16, p. 385–405, [https://doi.org/10.1016/S0743-9547\(98\)00022-1](https://doi.org/10.1016/S0743-9547(98)00022-1).
- Kang, D., Shen, W., Ning, J., and Ritzwoller, M.H., 2016, Seismic evidence for lithospheric modification associated with intracontinental volcanism in northeastern China: *Geophysical Journal International*, v. 204, p. 215–235, <https://doi.org/10.1093/gji/ggv441>.
- Key, K., Constable, S., Liu, L., and Pommier, A., 2013, Electrical image of passive mantle upwelling beneath the northern East Pacific Rise: *Nature*, v. 495, p. 499–502, <https://doi.org/10.1038/nature11932>.
- Konter, J.G., and Becker, T.W., 2012, Shallow lithospheric contribution to mantle plumes revealed by integrating seismic and geochemical data: *Geochemistry Geophysics Geosystems*, v. 13, Q02004, <https://doi.org/10.1029/2011GC003923>.
- Laumonier, M., Gaillard, F., Muir, D., Blundy, J., and Unsworth, M., 2017, Giant magmatic water reservoirs at mid-crustal depth inferred from electrical conductivity and the growth of the continental crust: *Earth and Planetary Science Letters*, v. 457, p. 173–180, <https://doi.org/10.1016/j.epsl.2016.10.023>.
- Li, B., Zhang, L., Guo, X., Li, W.C., and Ni, H., 2020a, Electrical conductivity of shoshonitic melts with application to magma reservoir beneath the Wudalianchi volcanic field, Northeast China: *Physics of the Earth and Planetary Interiors*, v. 306, 106545, <https://doi.org/10.1016/j.pepi.2020.106545>.
- Li, S., Weng, A., Li, J., Shan, X., Han, J., Tang, Y., Zhang, Y., and Wang, X., 2020b, Deep origin of Cenozoic volcanoes in Northeast China revealed by 3-D electrical structure: *Science China, Earth Sciences*, v. 63, p. 533–547, <https://doi.org/10.1007/s11430-018-9537-2>.
- Li, S.G., et al., 2017, Deep carbon cycles constrained by a large-scale mantle Mg isotope anomaly in eastern China: *National Science Review*, v. 4, p. 111–120, <https://doi.org/10.1093/nsr/nww070>.
- Liu, X., Fu, X., Liu, D., Wei, W., Lu, X., Liu, C., Wang, W., and Gao, H., 2018, Distribution of mantle-derived CO₂ gas reservoir and its relationship with basement faults in Songliao Basin, China: *Journal of Natural Gas Science and Engineering*, v. 56, p. 593–607, <https://doi.org/10.1016/j.jngse.2018.06.040>.
- Ma, J., Tian, Y., Zhao, D., Liu, C., and Liu, T., 2019, Mantle dynamics of western Pacific and East Asia: New insights from P wave anisotropic tomography: *Geochemistry Geophysics Geosystems*, v. 20, p. 3628–3658, <https://doi.org/10.1029/2019GC008373>.
- Massuyeau, M., Gardés, E., Rogerie, G., Aulbach, S., Tappe, S., Le Trong, E., Sifré, D., and Gaillard, F., 2021, MAGLAB: A computing platform connecting geophysical signatures to melting processes in Earth's mantle: *Physics of the Earth and Planetary Interiors*, v. 314, 106638, <https://doi.org/10.1016/j.pepi.2020.106638>.
- Pang, G., Feng, J., and Lin, J., 2016, Crust structure beneath Jilin Province and Liaoning Province in China based on seismic ambient noise tomography: *Journal of Volcanology and Geothermal Research*, v. 327, p. 249–256, <https://doi.org/10.1016/j.jvolgeores.2016.08.007>.
- Qin, X., Xu, Y., Zhang, H., Yu, S., and Qiu, H., 2008, Petrogenetic diversity of continental subalkaline volcanic rocks: An example from the Dunhua-Mishan-Dongning volcanic belt: *Acta Petrologica Sinica (Yanshi Xuebao)*, v. 24, p. 2501–2514 [in Chinese with English abstract].
- Sifré, D., Gardés, E., Massuyeau, M., Hashim, L., Hier-Majumder, S., and Gaillard, F., 2014, Electrical conductivity during incipient melting in the oceanic low-velocity zone: *Nature*, v. 509, p. 81–85, <https://doi.org/10.1038/nature13245>.
- Smith, I.E.M., and Németh, K., 2017, Source to surface model of monogenetic volcanism: A critical review, in Németh, K., et al., eds., *Monogenetic Volcanism: Geological Society [London] Special Publication 446*, p. 1–28, <https://doi.org/10.1144/SP446.14>.
- Suo, K., Zhang, G., Jiang, G., and Xu, Y., 2015, 3-D density distribution of the crust and upper mantle beneath Northeast China by joint inversion of gravity and seismic data: *Chinese Journal of Geophysics*, v. 58, p. 2436–2444, <https://doi.org/10.6038/cjg20150720> [in Chinese with English abstract].
- Wannamaker, P.E., Caldwell, T.G., Jiracek, G.R., Maris, V., Hill, G.J., Ogawa, Y., Bibby, H.M., Bennie, S.L., and Heise, W., 2009, Fluid and deformation regime of an advancing subduction system at Marlborough, New Zealand: *Nature*, v. 460, p. 733–736, <https://doi.org/10.1038/nature08204>.
- Wei, H., et al., 2003, Three active volcanoes in China and their hazards: *Journal of Asian Earth Sciences*, v. 21, p. 515–526, [https://doi.org/10.1016/S1367-9120\(02\)00081-0](https://doi.org/10.1016/S1367-9120(02)00081-0).
- Xu, M., Li, Y., Hou, H., Wang, C., Gao, R., Wang, H., Han, Z., and Zhou, A., 2017, Structural characteristics of the Yilan-Yitong and Dunhua-Mishan faults as northern extensions of the Tancheng-Lujiang fault zone: New deep seismic reflection results: *Tectonophysics*, v. 706–707, p. 35–45, <https://doi.org/10.1016/j.tecto.2017.03.018>.
- Xu, W.-L., Chen, J.-H., Weng, A.-H., Tang, J., Wang, F., Wang, C.-G., Guo, P., Wang, Y.-N., Yang, H., and Sorokin, A.A., 2020, Stagnant slab front within the mantle transition zone controls the formation of Cenozoic intracontinental high-Mg andesites in northeast Asia: *Geology*, v. 49, p. 19–24, <https://doi.org/10.1130/G47917.1>.
- Yan, J., and Zhao, J.X., 2008, Cenozoic alkali basalts from Jingpohu, NE China: The role of lithosphere-asthenosphere interaction: *Journal of Asian Earth Sciences*, v. 33, p. 106–121, <https://doi.org/10.1016/j.jseas.2007.11.001>.
- Zhang, Y., Wang, C., and Jin, Z., 2020, Decarbonation of stagnant slab in the mantle transition zone: *Journal of Geophysical Research: Solid Earth*, v. 125, p. e2020JB019533, <https://doi.org/10.1029/2020JB019533>.
- Zhang, Z., Lin, Z., Li, Z., Li, S., Li, Z., and Wang, X., 2000, Extreme mantle heterogeneity beneath the Jingpohu area, northeastern China—Geochemical evidence of Holocene basaltic rock: *Acta Geologica Sinica (English Edition)*, v. 74, p. 163–175, <https://doi.org/10.1111/j.1755-6724.2000.tb00445.x>.

Printed in USA